Supplementary Materials: Dynamics of Weakly Magnetic Nanoparticle Suspensions Near a Magnetized Sphere

Mohd Bilal Khan,[1,2] Abigail Patterson,[1,2] Jamel Ali,[1,2] Theo Siegrist,[1,2] Munir Humayun,[2,3] and Hadi Mohammadigoushki[1,2,a)]

[1)] *Department of Chemical and Biomedical Engineering, FAMU-FSU College of Engineering, Tallahassee, FL, 32310, USA*

[2)] *Center for Rare Earths, Critical Minerals, and Industrial Byproducts, National High Magnetic Field Laboratory, Tallahassee, FL 32310, USA*

[3)] *Department of Earth, Ocean and Atmospheric Science, Florida State University, Tallahassee, FL 32304, USA.*

(Dated: 29 May 2026)

[a)]Corresponding author; Electronic mail: hadi.moham@eng.famu.fsu.edu

I. ANALYTICAL MODEL FOR MAGNETIC FIELD DISTRIBUTION AROUND A SPHERE

For the sphere, the spatial distribution of the magnetic flux density $\mathbf{B}$ and the corresponding magnetic gradient $(\mathbf{B}\cdot\nabla)\mathbf{B}$ along the symmetry axis are obtained analytically by modeling the sphere as uniformly magnetized in a uniform applied field. We evaluate the field on the axis starting from the sphere surface, $x = 0$ and the axial distance from the sphere center is $r = R+x$, where R is the sphere radius. The applied magnetic field strength is $H_0 = B_0/\mu_0$, and the magnetic factor K which defines how strongly the sphere magnetizes relative to the surrounding medium under an applied magnetic field, is expressed as:

$$K = \frac{\mu_r - 1}{\mu_r + 2} \tag{1}$$

where μ_r is the effective relative permeability of the sphere material. The axial distribution of the field is:

$$B_{x,\mathrm{ind}}(r) = \frac{\mu_0}{4\pi}\frac{2m}{r^3} \tag{2}$$

Where m is the magnetic dipole moment. For a uniformly magnetized sphere, the dipole moment is given by:

$$m = \frac{4}{3}\pi a^3 M, \tag{3}$$

where a is the sphere radius and M is the magnetization. For a linear magnetic material subjected to an external field B_0, the magnetization can be expressed as

$$M = \frac{3K}{\mu_0}B_0 \tag{4}$$

so that the dipole moment becomes

$$m = \frac{4\pi a^3 K}{\mu_0}B_0 \tag{5}$$

The total axial flux density used for validation is

$$B_x(r) = B_0 + B_{x,\mathrm{ind}}(r) \tag{6}$$

and the axial gradient is obtained by differentiating the analytical expression. Finally, the magnetic gradient term along the axis is computed as:

$$(\mathbf{B}\cdot\nabla)\mathbf{B} \;\approx\; B_x\,\frac{dB_x}{dx} \tag{7}$$

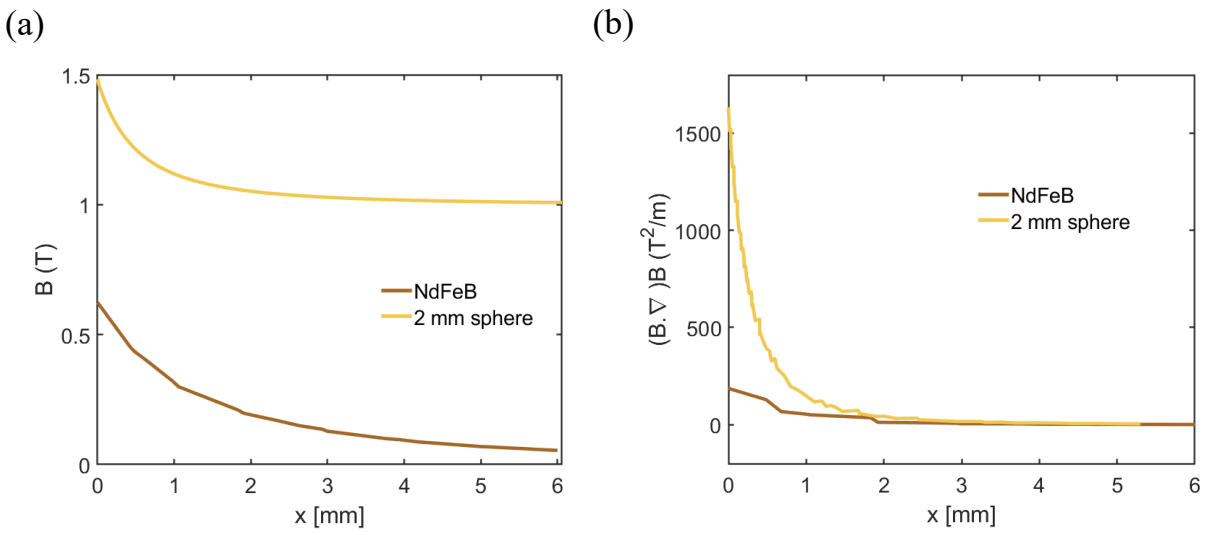

FIG. S1. Comparison of the (a) magnetic flux density and (b) magnetic field gradient distribution generated by an NdFeB permanent magnet and a stainless steel sphere with a diameter of 2 mm.

II. CALIBRATION CURVE

To assess the concentration variation within the experimental domain, we measured the absorbance intensity (light intensity) at a given concentration. Fig S2 shows the normalized absorbance intensity as a function of the concentration measured for all nano-particles used in this study. In here I is the intensity of the sample that has a solution and I_o is the background intensity (without sample). Clearly, the normalized light intensity shows a linear dependency with respect to the initial particle concentration, which is consistent with the Beer-Lambert law.

$$-log(I/I_o) = A \tag{8}$$

The linear fit regression has been performed by the relationship between absorbance (A) and concentration (c_0) as:

$$A = mc_0 + b \tag{9}$$

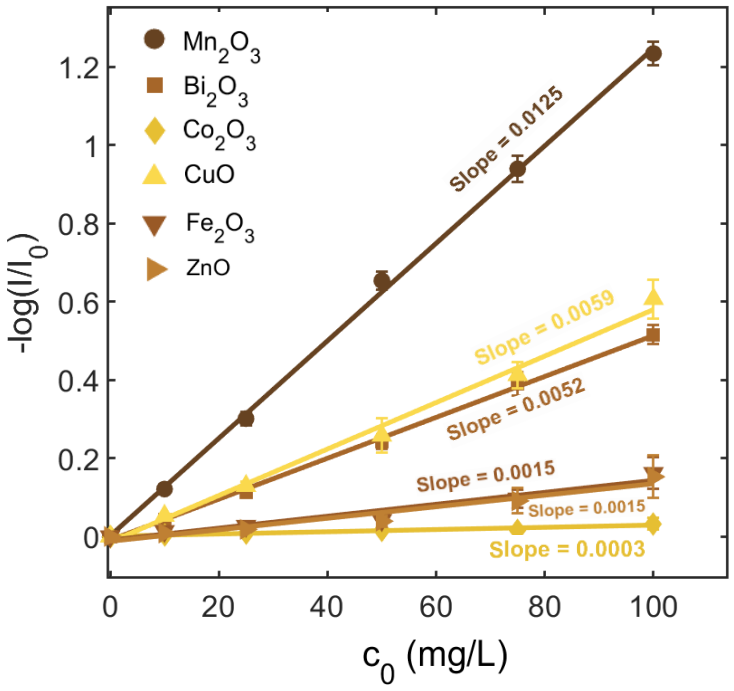

FIG. S2. Normalized absorbance intensity as a function of initial nanoparticle concentration for all the nanoparticles considered in this study. These graphs serve as calibration curves that are used in further analysis of the spatio-temporal evolution of particle concentration under the influence of an external magnetic field.

III. GOVERNING EQUATIONS FOR MULTIPHYSICS MODEL

A. Static magnetic field

Before simulating the magnetophoresis of nano-particles, it is important to simulate and validate the magnetic field distribution inside the cuvette, particularly in the vicinity of the stainless steel sphere. To simulate the static magnetic field, we use Maxwell-Ampère's law:

$$\nabla \times \mathbf{H} = \mathbf{A}; \tag{10}$$

Where $\mathbf{H}$ and $\mathbf{A}$ are the strength of the magnetic field and the current density, respectively. Another important equation is the Gauss law and constitutive relation for the magnetization that allows us to determine the magnetic flux density within the domain:

$$\nabla \cdot \mathbf{B} = 0; \mathbf{B} = \mu_0 \mu_r \mathbf{H}. \tag{11}$$

Here μ_0 is the permeability of free space, and μ_r is the relative permeability.

B. Mass and momentum balance

To analyze the transport of nanoparticles in the bulk fluid, we apply a force balance to the particle and fluid elements. The convective motion of the fluid element is governed by the continuity and the Navier-Stokes equations. To incorporate the effect of a magnetic dipole, a magnetic body force term, $\mathbf{F}_m = \frac{\chi_f}{\mu_0}(\mathbf{B}\cdot\nabla)\mathbf{B}$), based on the Kelvin force is introduced into the momentum equation, which influences both the nanoparticles and the surrounding fluid by transferring momentum through particle–fluid interactions as[1–3]:

$$\nabla\cdot\mathbf{u_f} = 0. \tag{12}$$

$$\rho\left[\frac{\partial\mathbf{u_f}}{\partial t} + \mathbf{u_f}\cdot\nabla\mathbf{u_f}\right] = \mu\nabla^2\mathbf{u_f} + (\rho-\rho_l)\mathbf{g} + \frac{\chi_f}{\mu_0}(\mathbf{B}\cdot\nabla)\mathbf{B}. \tag{13}$$

Here, $\mathbf{u_f}$, ρ, ρ_l, $\mathbf{g}$ and χ_f denote the fluid velocity, solution containing particle density, solvent density, gravitational acceleration and the volumetric magnetic susceptibility of the fluid element. In the case of a neutrally charged magnetic particle, its motion is governed by a force balance in the absence of inertia (Stokes' regime), which can be expressed as:

$$\mathbf{F}_{mp} + \mathbf{F}_d + \frac{4\pi R_p^3}{3}(\rho-\rho_l)\mathbf{g} = 0. \tag{14}$$

Here $\mathbf{F}_{mp}$ and $\mathbf{F}_d$ are the Kelvin and the drag force that the particle experiences in the solution, which are expressed as:

$$\mathbf{F}_{mp} = \frac{4\pi}{3}\frac{\Delta\chi R_p^3 c}{\mu_0}(\mathbf{B}\cdot\nabla)\mathbf{B}; \qquad \mathbf{F}_d = -6\pi\eta R_p\mathbf{v}_{mig}. \tag{15}$$

In the above equations, $\Delta\chi$ is the molar magnetic susceptibility difference between the particle and the surrounding fluid, R_p is the particle radius, c is the particle concentration in the fluid, and $\mathbf{v}_{mig}$ is the magnetophoretic velocity of the particle relative to the fluid element. The magnetophoretic velocity can be obtained by applying the force balance ($\mathbf{F}_{mp}-\mathbf{F}_d = 0$) as:

$$\mathbf{v}_{mig} = \frac{2R_p^3\,\rho\,\chi\,V}{9\mu_0\,\eta\,R_h}\,(\mathbf{B}\cdot\nabla)\mathbf{B} \tag{16}$$

The mass transport dynamics of the particles is given by a convective-diffusive equation expressed as:

$$\frac{\partial c}{\partial t} + \nabla\cdot\mathbf{N} = 0 \tag{17}$$

Here, $\mathbf{N}$ is the total molar flux of the particles presented as: $\mathbf{N} = -D\nabla c + c(\mathbf{u}_f + \mathbf{v}_{mig})$, with D being the diffusion coefficient of the particles in the fluid. A no-slip boundary condition is set to all the walls of the cuvette and the sphere surface. To account for particle capture in a cuvette caused by magnetophoresis and sedimentation, the flux at the cuvette walls and

sphere surface, $\mathbf{N}_b$, was defined as follows:

$$\mathbf{N}_b = \left[\frac{2R_p^2\Delta\chi}{9\mu_0\eta}c(\mathbf{B}.\nabla)\mathbf{B} + \frac{2R_p^2\nabla\rho}{9\eta}c\mathbf{g}\right].\mathbf{n} \tag{18}$$

Here $\mathbf{n}$ is the normal outward vector at the boundary. The flow in the domain is assumed to be inertialess because the particle Reynolds number is calculated to be $Re << 1$. By solving Eq. (10-17), in the computational domain, we can determine the magnetophoretic behavior of the particles around the sphere and the results will be compared with the experimental observations.

IV. PARTICLE SIZE DISTRIBUTION OF INITIAL SUSPENSION

A. Particle sedimentation under no magnetic field

To establish a baseline for particle dynamics in the absence of an external magnetic field, we first investigate the sedimentation-driven transport of nanoparticles under gravity alone. Fig. S3 (a) and (c) depict the spatiotemporal evolution of paramagnetic (Mn_2O_3) and and diamagnetic (Bi_2O_3) nanoparticles, as observed experimentally (top row) and captured through numerical simulations (bottom row). Due to gravitational settling, a vertical concentration gradient develops along the height of the cuvette, characterized by particle depletion at the top and accumulation near the bottom of the cuvette. To study the change in particle concentration within the domain, we define a dimensionless average concentration, $\langle c\rangle/c_0$, where $\langle c\rangle$ denotes the spatially averaged particle concentration at a given time, and c_0 is the initial uniform concentration. Moreover, Fig. S3 (b) and (d) present the temporal evolution of the averaged normalized concentration at various initial concentrations. As expected, sedimentation progressively reduces the bulk particle concentration in a cuvette. Furthermore, higher initial concentrations lead to a more effective depletion rate for both paramagnetic and diamagnetic nanoparticles. Nevertheless, the sedimentation process remains relatively slow: after 2 hours, around 2.5 % Mn_2O_3 and around 3.5% of Bi_2O_3 (diamagnetic) nanoparticles are removed from suspension. According to the manufacturer, the particle radii are 50 nm for Mn_2O_3 and 40 nm for Bi_2O_3. However, initial simulations conducted using these nominal sizes significantly underestimated the observed spatiotemporal evolution of particle concentration, as indicated by the dashed lines in Fig. S3 (b) and (d). To reconcile this mismatch, a polydisperse model incorporating three distinct particle size classes was introduced into the simulations, represented by the weighted sum $\sum_{i=1}^{3}\phi_i R_{pi}$, where ϕ_i and R_{pi} the radius of the i-th particle class. The particle radii and their corresponding mass fractions were systematically adjusted to achieve optimal agreement with the experimental measurements, as shown by the continuous lines in Fig. S3 (b) and (d). The resulting size distributions that produced the best fits are summarized in Table I. This deviation from the vendor-reported particle sizes is likely attributed to the formation of nanoparticle aggregates under experimental conditions.

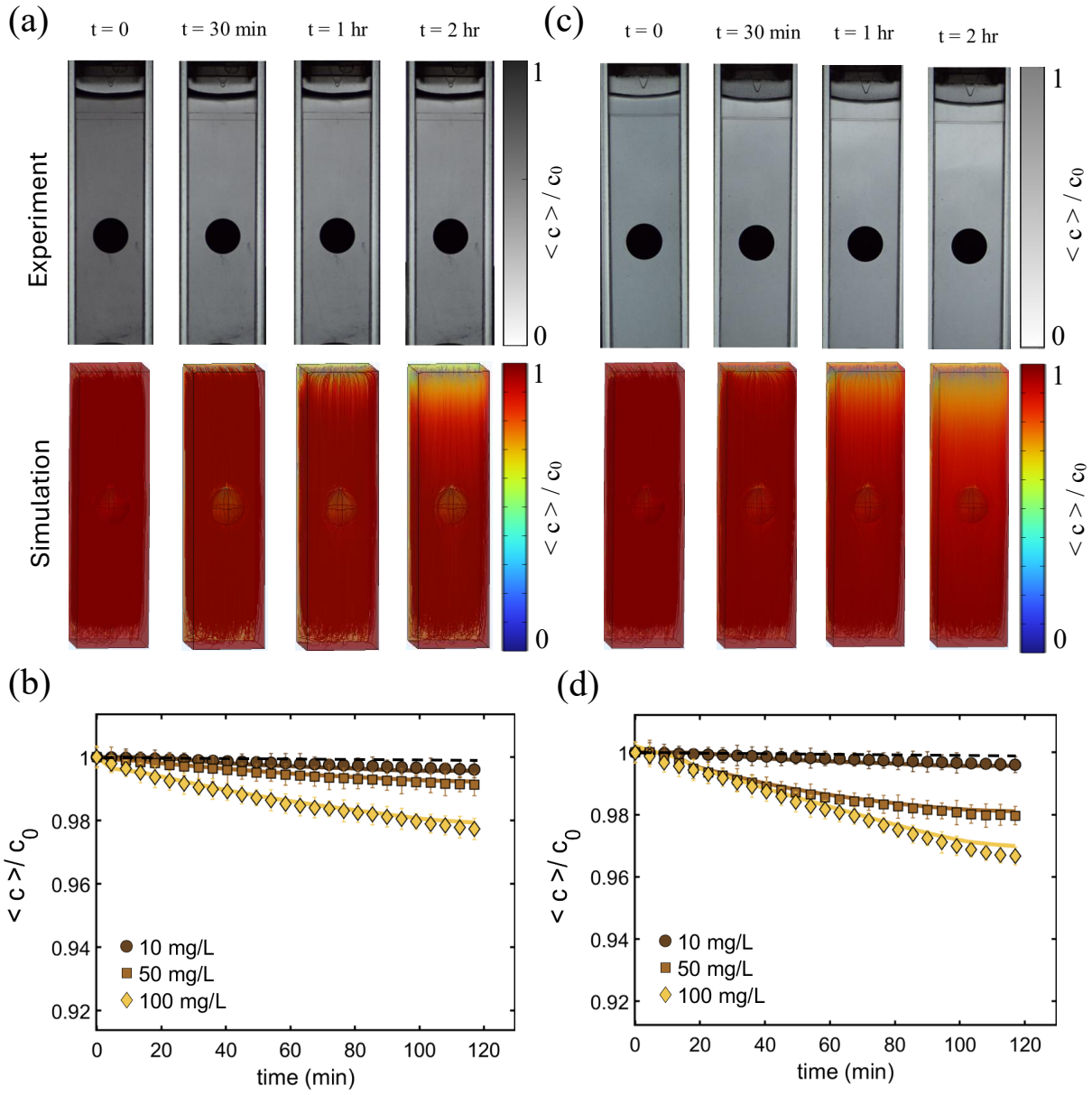

FIG. S3. Control experiments to assess particle sedimentation rate. The spatio-temporal evolution of (a) Mn_2O_3, and (c) Bi_2O_3 nano-particle concentrations as measured in experiments at an initial concentration of 100 [mg/L], magnetic field $\mathbf{B_0} = 0$ [T] and sphere diameter $d = 5$ [mm] (top row) and calculated through numerical simulations (bottom row). The averaged normalized concentration of Mn_2O_3 (b), and Bi_2O_3 (d) corresponding to part (a,c) for experimental data (symbols) and numerical simulation results (lines) for different initial concentrations. Note that the dashed line denotes the simulation results for vendor provided nano-particle size.

B. Dynamic light scattering (DLS)

The DLS of the nanoparticle samples was performed using an ALV/LSE-5004 light scattering instrument to determine the size distribution of the nanoparticles in solution. Measurements

TABLE I. Particle size distribution for simulations performed for $\mathbf{B_0} = 0$ T condition.

c_0 [mg/L]	$\mathbf{Mn_2O_3}$		$\mathbf{Bi_2O_3}$	
	ϕ_i	R_{pi} [nm]	ϕ_i	R_{pi} [nm]
10	0.84 0.10 0.06	50 100 150	0.84 0.10 0.06	40 80 120
50	0.83 0.10 0.07	50 100 150	0.82 0.10 0.08	40 80 120
100	0.80 0.10 0.10	50 150 200	0.80 0.12 0.08	80 120 160

were taken at angles ranging from 30° to 135°, in 15° steps. The measured particle sizes for all the metal oxides used in this study are presented in Table II.

TABLE II. Measured particle size and polydispersity index of different metal oxide nanoparticles in a solution.

Nanoparticle	$R_{p,DLS}$ **(nm)**	**Polydispersity Index**
Mn_2O_3	319.91	0.315
Fe_2O_3	432.255	0.326
Co_2O_3	445.245	0.363
CuO	662.57	0.343
Bi_2O_3	226.525	0.263
ZnO	213.985	0.230

V. ADDITIONAL DETAILS ON SCALING ANALYSIS

Consider the steady-state convection-diffusion equation for the nano-particle concentration $c(\mathbf{r})$ in the presence of a magnetophoretic drift velocity $\mathbf{v}_{mig}$:

$$\nabla \cdot \Big(- D\nabla c + c\mathbf{v}_{mig} \Big) = 0, \tag{19}$$

where D is the particle diffusion coefficient. For a radially symmetric capture problem around a sphere of radius a, this equation reduces to

$$\frac{1}{r^2}\frac{d}{dr}\left[r^2 \left(-D\frac{dc}{dr} + c\, v_{mig}(r) \right) \right] = 0, \tag{20}$$

where r is the distance from the sphere center. Integrating once gives the inward radial flux:

$$-D\frac{dc}{dr} + c\, v_{mig}(r) = \frac{J}{r^2}, \tag{21}$$

where J is the total inward particle flux. At the characteristic capture radius r_c, the concentration varies from c_0 (bulk) to ~ 0 (adsorbing surface). The concentration gradient scales as

$$\frac{dc}{dr} \sim \frac{c_0}{r_c}. \tag{22}$$

Therefore, the diffusive flux then scales as

$$J_D \sim D\frac{c_0}{r_c}. \tag{23}$$

The magnetic flux scales as

$$J_m \sim c_0\, v_{mig}(r_c). \tag{24}$$

By definition, the capture radius r_c is where these fluxes are comparable:

$$J_D \sim J_m \quad \Rightarrow \quad D\frac{c_0}{r_c} \sim c_0\, v_{mig}(r_c). \tag{25}$$

Canceling c_0 yields $v_{mig}(r_c) \sim \frac{D}{r_c}$.

Including this relation (i.e., $v_{mig}(r_c) \sim \frac{D}{r_c}$) into the Eqs. (4-5) of the manuscript leads to:

$$\frac{D}{r_c} \sim \frac{V_p \Delta\chi_v}{\mu_0}\frac{B_0^2 a^6}{r_c^7}. \tag{26}$$

Rearranging the above equation to obtain r_c leads to $r_c \sim B_0^{1/3} a$.

FIG. S4. Spatio-temporal evolution of (a) Mn_2O_3, and (b) Bi_2O_3 nano-particle concentrations as a function of sphere diameters at a fixed concentration of 100 mg/L, and a magnetic field of 1 T.

VI. MAGNETIC SEPARATION WITHOUT HYDRODYNAMIC INTERACTION

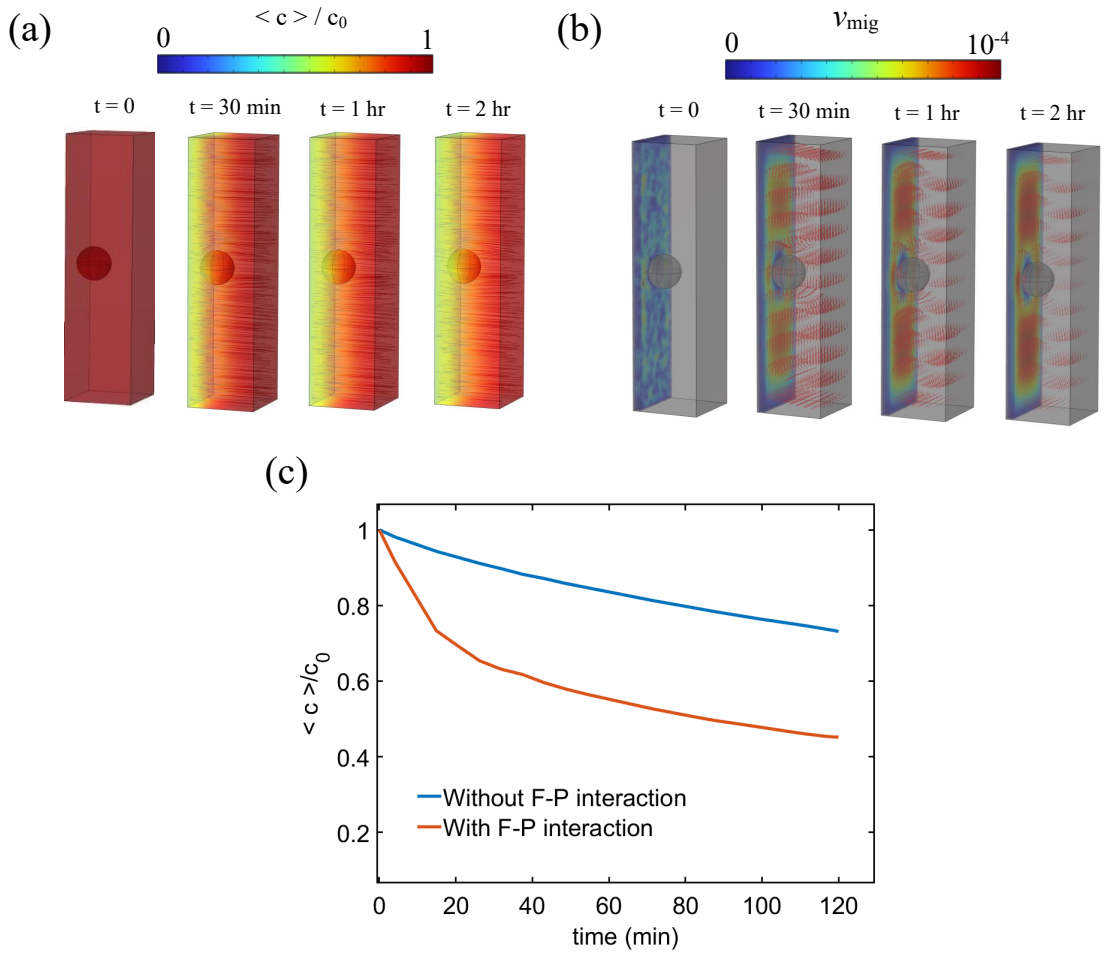

FIG. S5. (a) The normalized concentration field for manganese oxide nanoparticles at a concentration = 100 mg/L, magnetic field $\mathbf{B_0} = 1$ T, and a sphere diameter, $d = 5$ mm, in the absence of fluid–particle interactions. (b) Corresponding particle velocity field (m/s) and (c) temporal evolution of the normalized average concentration for simulations without fluid-particle (F-P) interaction, and with fluid-particle (F-P) interaction. Without F-P interactions, approximately 28% of the particles are captured after 2 hours, significantly less than the $\sim 55\%$ separation achieved when hydrodynamic interactions are included in the separation. This comparison revealed the crucial role of hydrodynamic coupling and flow-induced effects in enhancing particle transport and improving the efficiency of magnetic separation.

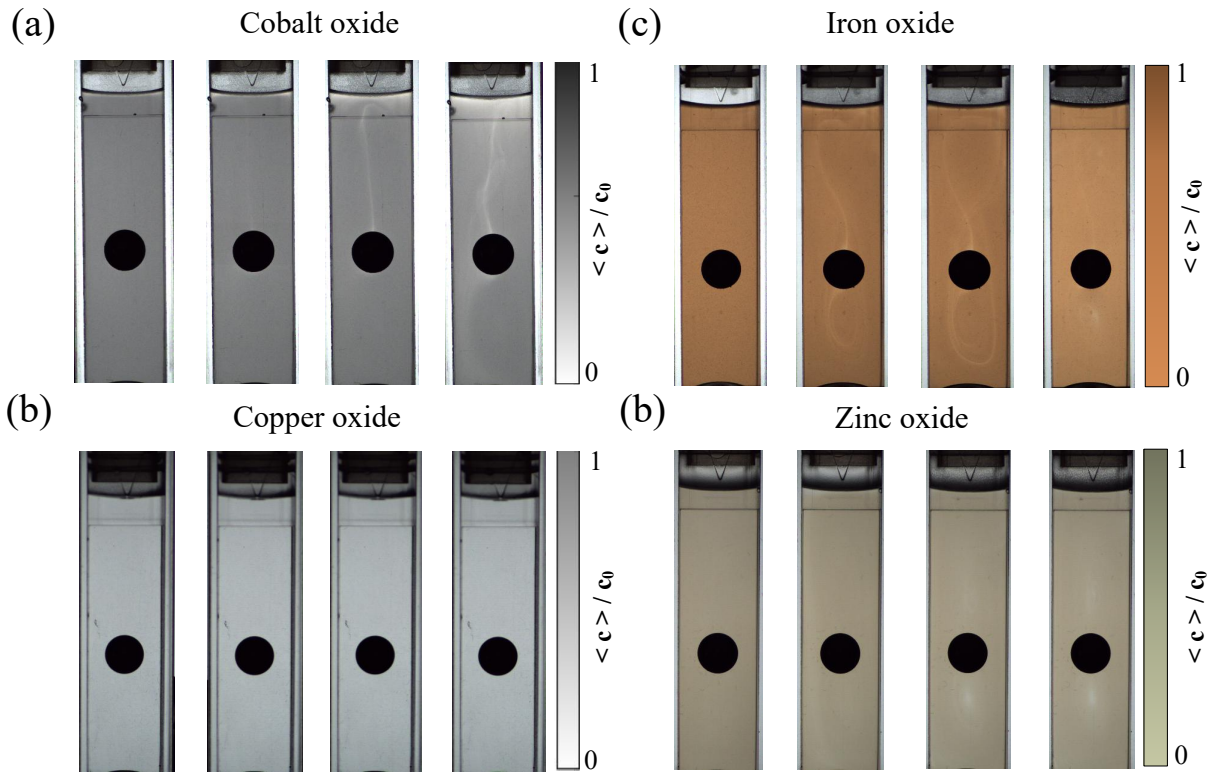

FIG. S6. The spatio-temporal evolution of (a) Co_2O_3, (b) Fe_2O_3, (c) CuO and (d) ZnO as a function of initial nanoparticle concentration of 100 mg/L, $\mathbf{B_0} = 1$ T and a sphere diameter $d =$ 5 mm.

REFERENCES

[1]Jie Huang, Donald D Gray, and Boyd F Edwards. Thermoconvective instability of paramagnetic fluids in a nonuniform magnetic field. *Physical Review E*, 57(5):5564, 1998.

[2]Peter Rassolov, Jamel Ali, Theo Siegrist, Munir Humayun, and Hadi Mohammadigoushki. Magnetophoresis of paramagnetic nanoparticles in suspensions under magnetic field gradients. *Physical Review Fluids*, 10(7):073701, 2025.

[3]Tim A Butcher and JMD Coey. Magnetic forces in paramagnetic fluids. *Journal of Physics: Condensed Matter*, 35(5):053002, 2023.